

Integration of Data and Theory for Accelerated Derivable Symbolic Discovery

Cristina Cornelio^{1,2}, Sanjeeb Dash¹, Vernon Austel¹,
Tyler Josephson^{3,4}, Joao Goncalves¹, Kenneth Clarkson¹,
Nimrod Megiddo¹, Bachir El Khadir¹, Lior Horesh^{1,◊}

¹IBM Research

²Samsung AI Center Cambridge

³Department of Chemical, Biochemical, and Environmental Engineering,
University of Maryland, Baltimore County

⁴Department of Chemistry and Chemical Theory Center, University of Minnesota

◊ Correspondence e-mail: lhoresh@us.ibm.com

One-Sentence Summary: Combining logical reasoning with symbolic regression enables principled derivation of laws of nature discovered in data.

Abstract: Scientists have long aimed to discover meaningful equations which accurately describe data. Machine learning algorithms automate construction of accurate data-driven models, but ensuring that these are consistent with existing knowledge is a challenge. We developed a methodology combining automated theorem proving with symbolic regression, enabling principled derivations of laws of nature. We demonstrate this for Kepler's third law, Einstein's relativistic time dilation, and Langmuir's theory of adsorption, in each case, automatically connecting experimental data with background theory. The combination of logical reasoning with machine learning provides generalizable insights into key aspects of the natural phenomena.

Main text:

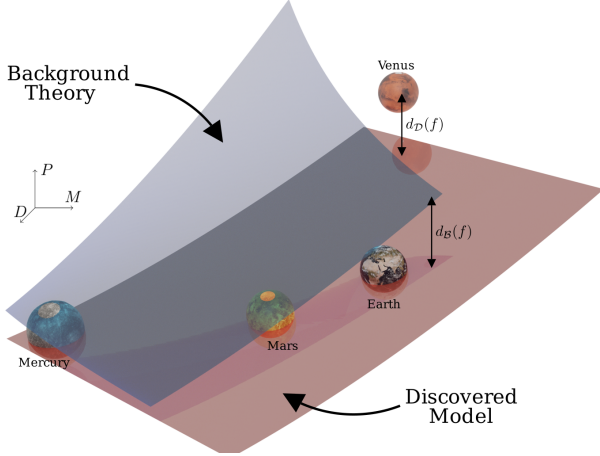
Introduction

Artificial neural networks (NN) and statistical regression are commonly used to automate the discovery of patterns and relations in data. NNs return “black-box” models, where the underlying functions are typically used for prediction only. In standard regression, the functional form is determined in advance, so model discovery amounts to parameter fitting. In symbolic regression (SR) [28, 29], the functional form is *not* determined in advance. It may apply operations from a given list, e.g., $+$, $-$, \times , and \div , so the functional form is calculated from the data. SR models are typically more “interpretable” than NN models, and require less data. For discovering laws of nature in symbolic form from experimental data, SR may work better than NNs or fixed-form regression [41]; integration of NNs with SR has been a topic of recent developments in neuro-symbolic AI [34, 25, 47]. However, a major challenge in SR is to identify, out of many models that fit the data, those that are *scientifically meaningful*. In [41], meaningful functions are identified as those which balance accuracy and complexity, but many such expressions exist for a given dataset, and not all are consistent with theory.

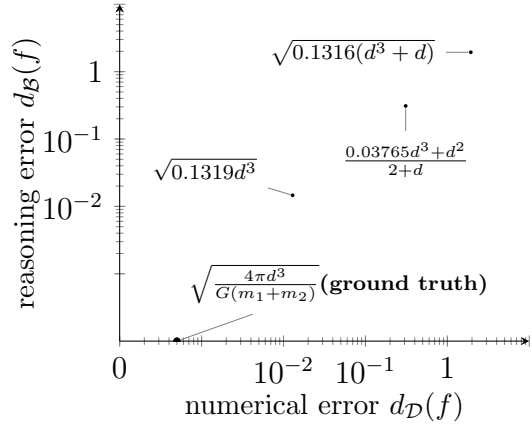
Deriving explainable models using automated theorem provers (ATP) is an open question. Generalized reasoners are challenged by computational complexity. One possible approach is enhancing ATP with machine learning techniques, e.g., using reinforcement learning to guide the search [17]. This research area has received much attention recently [39, 8, 20], and even deep-learning and reinforcement-learning methods have been developed, albeit with very limited logic expressivity. This task is further challenged by the lack of appropriate datasets. Moreover, deriving models from background theory using formal logical-reasoning tools is especially difficult when arithmetic and calculus operators are required.

Models which are derivable, and not merely empirically accurate, are appealing because they are arguably correct, predictive, and insightful. We attempt to obtain these by combining a novel mathematical-optimization-based SR method with a reasoning system. This yields an end-to-end discovery system, which furnishes either a formal proof of derivability of the extracted formula from a set of axioms, or a proof of inconsistency. We present novel measures that indicate how close a formula is to a derivable formula, when the model is provably non-derivable, and we calculate the values of these measures using our reasoning system.

To the best of our knowledge, there is limited work combining SR with ATP. The authors of [33] use a logic-based description to constrain the output of a GAN neural architecture for generating images. In [42, 5], machine-learning tools and reasoning engines



(a) A visual representation of the numerical data, background theory, and the discovered model $P = f(d, M) = \sqrt{0.1319d^3}$. dataset. The grey surface represents solutions of the background-theory equations. The red surface is the graph of the discovered model f . The double arrows indicate the distances $d_B(f)$ and $d_D(f)$.



(b) Depiction of symbolic models produced by our SR system by points (x, y) , where x represents distance to data, and y represents distance to background theory. Both distances are computed with an appropriate norm.

Figure 1: Depiction of symbolic models for Kepler's third law of planetary motion giving the orbital period a planet around a star. The data consists of measurements (m_1, m_2, d, P) of the mass of the sun m_1 , the orbital period P and mass m_2 for each planet and its distance d from the sun. The background theory amounts to Newton's laws of motion, i.e., the equations for kinetic force, gravitational force, and equilibrium conditions. 4-tuples (m_1, m_2, d, P) are projected into $(m_1 + m_2, d, P)$.

are combined to augment the initial dataset with new points in order to improve efficiency of learning methods and the fidelity of the final model to known theory.

Methodology

Our automated scientific discovery method aims to discover an unknown *symbolic model* $y = f(\mathbf{x})$ where \mathbf{x} is the vector¹ (x_1, \dots, x_n) of independent variables, and y is the dependent variable. The model should fit a collection of m data points, $((\mathbf{X}^1, Y^1), \dots, (\mathbf{X}^m, Y^m))$, be derivable from a background theory, and should have low complexity and bounded prediction error. More specifically, the inputs to our system are triples $\langle \mathcal{B}, \mathcal{C}, \mathcal{D} \rangle$ as follows.

Background Knowledge \mathcal{B} , a set of domain-specific axioms expressed as logic formulas². They involve \mathbf{x} , and y , and possibly more variables that are necessary to formulate the background theory. **A Hypothesis Class** \mathcal{C} , a set of admissible symbolic models defined by a grammar and a set to invariance constraints to avoid redundant expressions (e.g., $A + B$ is equivalent to $B + A$). **Data** \mathcal{D} , a set of m examples, each providing certain values for x_1, \dots, x_n , and y .

In general, there may not exist an $f \in \mathcal{C}$ that fits the data exactly and is derivable from \mathcal{B} . This could happen because the symbolic model generating the data might not belong to \mathcal{C} , the sensors used to collect the data might give noisy measurements, or the background knowledge might be inaccurate or incomplete. To quantify the compatibility of a symbolic model with data and background theory, we introduce the notion of *distance* between a model f and \mathcal{B} . Roughly, it reflects the distance between the predictions of f and the predictions of \mathcal{B} , and equals zero when f is derivable from \mathcal{B} ; a precise definition is given below. Figures 1a and 1b provide a visualization of these two notions of distance for the problem of learning Kepler’s third law from data and background theory.

The output is a list of candidate symbolic models that fit the data. For each model, the system outputs the distance $d_{\mathcal{D}}(f)$ between f and \mathcal{D} and the distance $d_{\mathcal{B}}(f)$ between f and \mathcal{B} .

Our system consists of an SR-module and a reasoning module. The SR-module returns multiple candidate models or formulae expressing y as a function of x_1, \dots, x_n . These models are passed to the reasoning module along with \mathcal{B} . The reasoning module tests each candidate for derivability. If a model is found to be derivable from \mathcal{B} , it is returned as the chosen model for prediction; otherwise, if the reasoning module concludes that no candidate model is derivable, it is necessary to either collect additional data or add constraints. In this case, the reasoning module will return a new ranking of the input set of candidate hypothesis, based on the distance $d_{\mathcal{B}}$. The reasoning module can prove that a model is not derivable by returning counterexample points that satisfy \mathcal{B} but do not fit the model.

¹Bold letters indicate vectors.

²In our implementation we focus on first-order-logic formulas with equality, inequality and basic arithmetic operators

Theory Discovery System

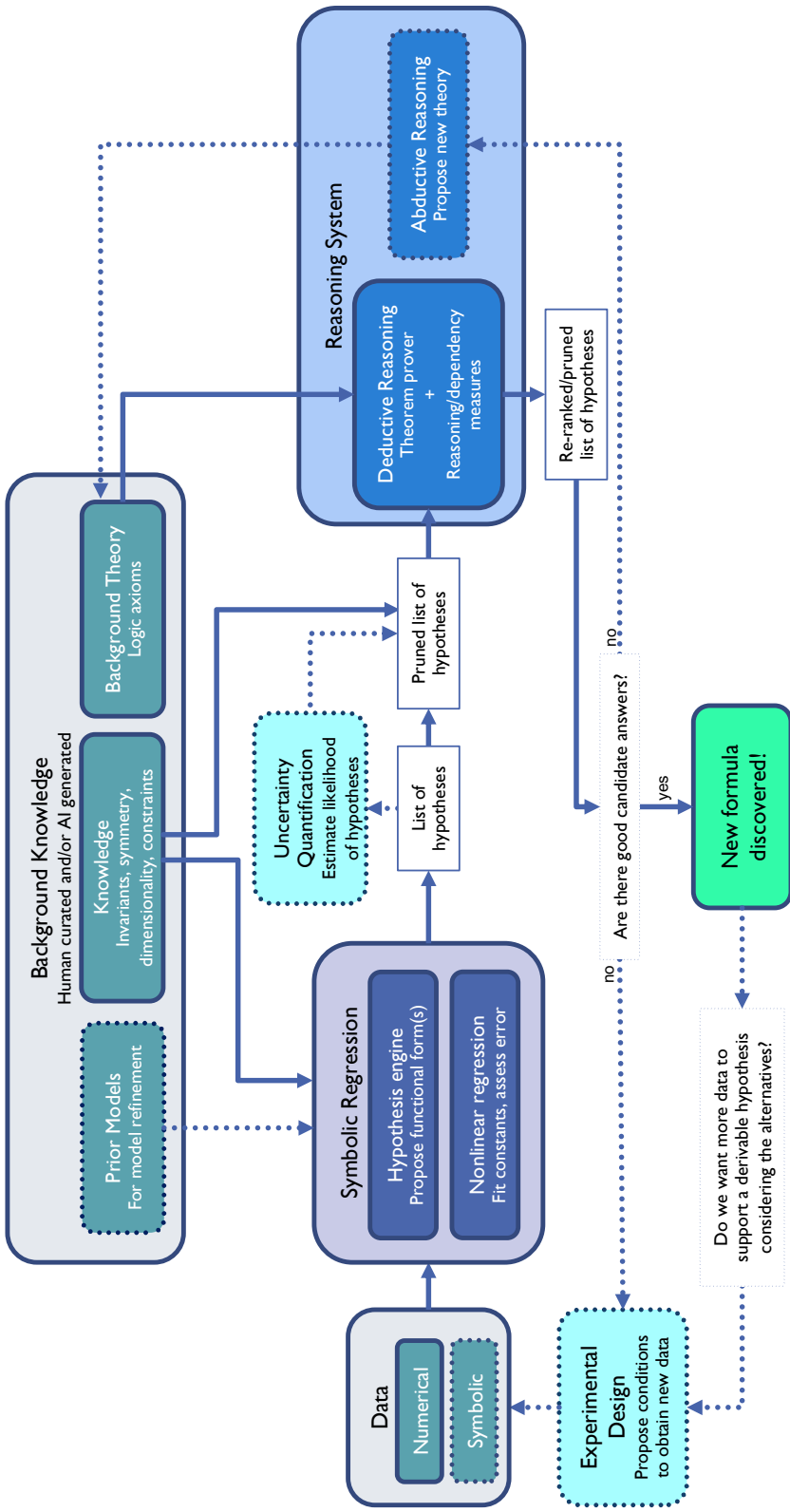


Figure 2: System overview. Solid lines and boundaries correspond to our system, and dashed lines and boundaries indicate standard techniques for scientific discovery (human-driven or artificial) that have not been integrated into the current system. The present system generates hypotheses from data using symbolic regression, which are posed as conjectures to an automated deductive reasoning system, which proves or disproves them based on background theory.

SR is mostly solved with genetic programming (GP) [28, 29, 6, 41], though mixed-integer nonlinear programming (MINLP)-based methods have recently been developed for SR [7, 14, 15]. We develop a new MINLP-based SR solver (described in the Appendix). The input consists of a subset of the operators $\{+, -, \times, \div, \sqrt{\cdot}, \log, \exp\}$, an upper-bound on expression complexity, and an upper-bound on the number of constants used that do not equal 1. Given a dataset, the system formulates multiple MINLP instances to find an expression that minimizes the least-squares error. Each instance is solved approximately subject to a time limit. Both linear and nonlinear constraints can be imposed. In particular, dimensional consistency is imposed when physical dimensions of variables are available.

We propose using the KeYmaera X reasoner [21], an ATP for hybrid systems, which combines different types of reasoning: deductive, real-algebraic, and computer-algebraic reasoning. We also propose using Mathematica [3] for certain types of analysis of symbolic expressions. While a formula found by any grammar-based system (such as a SR system) is syntactically correct, it may be in contradiction with the axioms of the theory, or may not be derivable from them. In some cases, if the formula is not derivable, the theory may not have enough axioms; the formula may be provable under an extended axiom set (possibly discovered by abduction). An overall schematic of the system is depicted in Figure 2 where the bold lines and boundaries correspond to the system we present in this work, and the dashed lines and boundaries refer to standard techniques for scientific discovery that we have not yet integrated into our current implementation.

Results

Here we describe experimental results for three problems to show the different capabilities of our system. First, we consider planetary motion data in order to derive Kepler’s third law of planetary motion, and provide reasoning-based measures to analyze the quality and generalizability of the generated formulas. Extracting this law from experimental data is challenging, especially when the masses involved are of very different magnitudes, as in the solar system where the solar mass is much larger than planetary masses. The reasoning module helps in choosing between different candidate formulae. We then consider Einstein’s time dilation formula. Though we do not recover this formula from data, we can use the reasoning module to identify the formula that generalizes best. Finally, we consider Langmuir’s adsorption equation, whose background theory contains material-dependent coefficients of proportionality, which cannot be easily calculated. Our system is able to connect numerical data with automated reasoning, while exploiting existentially-quantified variables representing unknown constants.

Kepler's third law of planetary motion.

Kepler's law relates the distance between two bodies, e.g., the sun and a planet in the solar system, and their orbital periods. It can be expressed as:

$$P = \sqrt{\frac{4\pi^2 d^3}{G(m_1 + m_2)}} \quad (1)$$

where P is the period, G is the gravitational constant, and m_1 and m_2 are the two masses. It can be derived using the following axioms, describing the center of mass (axiom K1), the distance between bodies (axiom K2), the gravitational force (axiom K3), the centrifugal force (axiom K4), the force balance (axiom K5), and the period (axiom K6):

$$\text{K1. } m_1 * d_1 = m_2 * d_2$$

$$\text{K2. } d = d_1 + d_2$$

$$\text{K3. } F_g = \frac{Gm_1m_2}{d^2}$$

$$\text{K4. } F_c = m_2d_2w^2$$

$$\text{K5. } F_g = F_c$$

$$\text{K6. } P = \frac{2\pi}{w}$$

$$\text{K7. } m_1 > 0, m_2 > 0, P > 0, d_1 > 0, d_2 > 0$$

We considered three real-world datasets: planets of the solar system,³ the solar-system planets along with exoplanets from Trappist-1 and the GJ 667 system,⁴ and binary-stars [38]. These datasets contain measurements of pairs of masses, a sun and a planet for the first two, and two suns for the third, the distance between them, and the orbital period of the planet around the sun in the first two datasets. The data we use is given in the Appendix. Note that the dataset does not contain measurements for a number of variables in the axiom system, such as d_1, d_2, F_g , etc. To avoid numerical errors in MINLP, we scale the numbers, e.g., masses of planets and stars, in each dataset and give the scaling/normalization factors in the Appendix. The goal is to recover Kepler's third law from the data, i.e., to obtain P as the above-stated function of d, m_1 and m_2 . The SR-module takes as input the set $\{+, -, \times, \div, \sqrt{\cdot}\}$.

None of the formulas obtained via SR are derivable, though some are close approximations to derivable formula. We evaluate the quality of these formulas by writing a logic program for calculating the relative error of a formula with respect to a derivable formula.

³<https://nssdc.gsfc.nasa.gov/planetary/factsheet/>

⁴NASA exoplanet archive <https://exoplanetarchive.ipac.caltech.edu/>

We present three metrics to assess the correctness of a data-driven from a reasoning viewpoint: *pointwise reasoning error*, *generalization reasoning error*, and *variable dependence*. Each metric assumes the availability of a complete (containing all the axioms necessary to that explain the phenomena under consideration comprehensively) and consistent (with no axioms in contradiction) background theory.

Pointwise reasoning error: The key idea is to compute a distance between a formula generated from the numerical data and some deducible formula that is implicitly defined by the axiom set. The distance is measured by the ℓ_2 or ℓ_∞ norm applied to the difference between the values of the numerically derived formula and a deducible formula at the points in the dataset. These results can be extended to other norms.

We compute the relative error of numerically derived formula $f(\mathbf{x})$ applied to the m data points \mathbf{X}^i ($i = 1, \dots, m$) with respect to some derivable formula $\tilde{f}(\mathbf{x})$ deducible from the axioms via the following expressions⁵:

$$\varepsilon(\ell_2) = \sqrt{\sum_{i=1}^m \left(\frac{f(\mathbf{X}^i) - \tilde{f}(\mathbf{X}^i)}{\tilde{f}(\mathbf{X}^i)} \right)^2} \quad \text{and} \quad \varepsilon(\ell_\infty) = \max_{1 \leq i \leq m} \left\{ \frac{|f(\mathbf{X}^i) - \tilde{f}(\mathbf{X}^i)|}{|\tilde{f}(\mathbf{X}^i)|} \right\}. \quad (2)$$

The KeYmaera formulation of these two measures for the first formula ($\sqrt{0.1319 \cdot d^3}$) of Table 1 can be found in the Appendix.

Table 1 reports in columns 5 and 6 the values of $\varepsilon(\ell_2)$ and $\varepsilon(\ell_\infty)$, respectively. It also reports the relative numerical errors in columns 3 and 4, measured by the ℓ_2 and ℓ_∞ norms respectively, for the candidate expressions given in column 2 when evaluated on the points in the dataset.⁶

The pointwise reasoning errors are not very informative if SR yields a low-error candidate expression (measured with respect to the data), and the data itself satisfies the background theory up to a small error, which indeed is the case with the data we use; the reasoning errors and numerical errors are very similar.

Generalization reasoning error: Even when one can find a function that fits given data points well, it is challenging to obtain a function that *generalizes* well, i.e., one which yields good results at points of the domain not equal to the data points. Let $\varepsilon(\ell_\infty)_S$ be calculated for a candidate formula $f(\mathbf{x})$ over a domain S that is not equal to the original set of data points as follows:

$$\varepsilon(\ell_\infty)_S = \max_{\mathbf{x} \in S} \left\{ \frac{|f(\mathbf{x}) - \tilde{f}(\mathbf{x})|}{|\tilde{f}(\mathbf{x})|} \right\}. \quad (3)$$

⁵ $\tilde{f}(\mathbf{X}^i)$ represent a derivable formula for the variable of interest y evaluated on the data points \mathbf{X}^i .

⁶We attempt to minimize absolute ℓ_2 error (and not relative error) when obtaining candidate expressions via symbolic regression.

This measure indicates how well our candidate function generalizes to all points in S ; however, the function $\tilde{f}(\mathbf{x})$ is not known and must be deduced from the axioms via a theorem prover; hence the name *relative generalization reasoning error*. If we do not divide by $\tilde{f}(\mathbf{x})$ in the above expression, we get the absolute version of this error metric. For the Kepler dataset, we let S be the smallest multi-dimensional interval (or Cartesian product of intervals on the real line) containing all data points. In column 7 of Table 1, we show the generalization reasoning error on the Kepler datasets with S defined as above. If this error is roughly the same as the pointwise reasoning error for ℓ_∞ , e.g., for the solar system dataset, then the formula extracted from the numerical data is as accurate at points in S as it is at the data points.

Variable dependence: In order to check if the functional dependence of a candidate formula on a specific variable is accurate, we compute the generalization error over a domain S where the domain of this variable is extended by an order of magnitude beyond the smallest interval containing the values of the variable in the dataset. Thus we can check whether there exist special conditions under which the formula does not hold. We modify an endpoint of an interval by one order of magnitude, one variable at a time. If we notice an increase in the generalization reasoning error while modifying intervals for one variable, we deem the candidate formula as missing a dependency on that variable. A missing dependency might occur because the exponent for a variable is incorrect, or that variable is not considered at all while it should be. One can get further insight into the type of dependency by analyzing how the error varies, e.g., linearly or exponentially. Table 1 provides in columns 8–10 results regarding the candidate formulas for Kepler’s third law. For each formula, the dependencies on m_1 , m_2 , and d are indicated by 1 or 0 (for correct or incorrect dependency). For example, the candidate formula $P = \sqrt{0.1319 \cdot d^3}$ for the solar system does not depend on either mass, and the dependency analysis suggests that the formula approximates well the phenomenon in the solar system, but not for larger masses. The best formula for the binary star dataset, $\sqrt{d^3}/(0.9967m_1 + m_2)$, has no missing dependency (all ones in columns 8–10), i.e., it generalizes well; increasing the domain along any variable does not increase the generalized reasoning error.

Relativistic time dilation.

Einstein’s theory of relativity postulates that the speed of light is constant and implies that two observers in relative motion to each other will experience time differently and observe different clock frequencies. The frequency f for a clock moving at speed v is

| | 1 | 2 | 3 | 4 | 5 | 6 | 7 | 8 | 9 | 10 |
|--------------|---|-------------------|-----------------|---------------|-------------------|---------------|------------------|--------------|-------|-----|
| Dataset | $P =$ | Candidate formula | numerical error | | point. reas. err. | | gen. reas. error | dependencies | | |
| | | | ℓ_2 | ℓ_∞ | ℓ_2 | ℓ_∞ | ℓ_∞ | m_1 | m_2 | d |
| solar | $\sqrt{0.1319 \cdot d^3}$ | | .01291 | .006412 | .0146 | .0052 | .0052 | 0 | 0 | 1 |
| | $\sqrt{0.1316 * (d^3 + d)}$ | 1.9348 | 1.7498 | 1.9385 | 1.7533 | 1.7559 | 0 | 0 | 0 | |
| | $(0.03765d^3 + d^2)/(2 + d)$ | .3102 | .2766 | .3095 | .2758 | .2758 | 0 | 0 | 0 | |
| exoplanet | $\sqrt{0.1319d^3/m_1}$ | .08446 | .08192 | .02310 | .0052 | .0052 | 0 | 0 | 1 | |
| | $\sqrt{m_1^2m_2^3/d + 0.1319d^3/m_1}$ | .1988 | .1636 | .1320 | .1097 | > 550 | 0 | 0 | 0 | |
| | $\sqrt{(1 - .7362m_1)d^3/2}$ | 1.2246 | .4697 | 1.2418 | .4686 | .4686 | 0 | 0 | 1 | |
| binary stars | $1/(d^2m_1^2) + 1/(dm_2^2) - m_1^3m_2^2 + \sqrt{.4787d^3/m_2 + d^2m_2^2}$ | .002291 | .001467 | .0059 | .0050 | timeout | 0 | 0 | 0 | |
| | $(\sqrt{d^3} + m_1^3m_2/\sqrt{d})/\sqrt{m_1 + m_2}$ | .003221 | .003071 | .0038 | .0031 | timeout | 0 | 0 | 0 | |
| | $\sqrt{d^3/(0.9967m_1 + m_2)}$ | .005815 | .005337 | .0014 | .0008 | .0020 | 1 | 1 | 1 | |

Table 1: Numerical error values, pointwise reasoning error values, and generalization error values for candidate solutions for the Kepler dataset. We also give an analysis of the variable dependence of candidate solutions. For simplicity of notation, in the table we use the variables d , m_1 , m_2 and P , while referring to the normalized counterparts, d_N , m_{1N} , m_{2N} and P_N .

related to the frequency f_0 of a stationary clock by the formula

$$\frac{f - f_0}{f_0} = \sqrt{1 - \frac{v^2}{c^2}} - 1 \quad (4)$$

where c is the speed of light. This formula was recently confirmed experimentally by Chou et. al. [13] using high precision atomic clocks. We test our system on the experimental data of [13] which consists of measurements of v and associated values of $(f - f_0)/f_0$, reproduced in the Appendix. We take the axioms for derivation of the time dilation formula from [10, 43]. These are also listed in the Appendix and involve variables that are not present in the experimental data.

In Table 2 we give some functions obtained by our SR module (using the operators $\{+, -, \times, \div, \sqrt{\}$ as input) along with the numerical errors of the associated functions and generalization reasoning errors. The 6th column gives the set S as an interval for v for which our reasoning module can verify that the absolute generalization reasoning error of the function in the first column is at most 1. The last column gives the interval for v for which we can verify a relative generalization reasoning error of at most 2%. Even though the last function has low relative error according to this metric, it can be ruled out as a reasonable candidate if one assumes the target function should be continuous (it has a singularity at $v = 1$). Thus, even though we cannot obtain the original function, we obtain another which generalizes well, as it yields excellent predictions for a very large

range of velocities.

| Candidate formula | Numerical Error | | Numerical Error | | Gen. Error $\ell_\infty \leq 1$ | Gen. Error $\ell_\infty \leq 0.02$ |
|--|----------------------|---------------------------|----------------------|---------------------------|------------------------------------|---------------------------------------|
| | Absolute ℓ_2 | Relative ℓ_∞ | Absolute ℓ_2 | Relative ℓ_∞ | | |
| $y = -.00563v^2$ | 0.3822 | 0.3067 | 1.081 | 0.001824 | $37 \leq v \leq 115$ | $37 \leq v \leq 10^8$ |
| $\frac{v}{1+.00689v} - v$ | 0.3152 | 0.2097 | 1.012 | 0.006927 | $37 \leq v \leq 49$ | $37 \leq v \leq 38$ |
| $-.00537 \frac{v^2 \sqrt{v+v^2}}{(v-1)}$ | 0.3027 | 0.2299 | 1.254 | 0.002147 | $37 \leq v \leq 98$ | $37 \leq v \leq 109$ |
| $-.00545 \frac{v^4}{\sqrt{v^2+v^{-2}}(v-1)}$ | 0.3238 | 0.2531 | 1.131 | 0.0009792 | $37 \leq v \leq 126$ | $37 \leq v \leq 10^7$ |

Table 2: Candidate functions derived from time dilation data, and associated error values

In this case, our system can also help rule out alternative axioms. Consider replacing the axiom that the speed of light is a constant value c by a “Newtonian” assumption that light behaves like other mechanical objects: if emitted from an object with velocity v in a direction perpendicular to the direction of motion of the object, it has velocity $\sqrt{v^2 + c^2}$. Replacing c by $\sqrt{v^2 + c^2}$ (in axiom R2 in the Appendix to obtain R2') produces a self-consistent axiom system (as confirmed by the theorem prover), albeit one leading to no time dilation. Our reasoning module concludes that none of the functions in Table 2 is compatible with this updated axiom system: the absolute generalization reasoning error is greater than 1 for any range $[37, r]$ where $r \geq 37$ (the pointwise reasoning error is also high). Consequently, the data is used indirectly to discriminate between axiom systems relevant for the phenomenon under study; SR poses only accurate formulas as conjectures.

Langmuir’s adsorption equation.

The Langmuir adsorption equation describes a chemical process in which gas molecules contact a surface, and relates the loading q on the surface to the pressure p of the gas⁷ [31]:

$$q = \frac{q_{\max} K_a \cdot p}{1 + K_a \cdot p}. \quad (5)$$

The constants q_{\max} and K_a characterize the maximum loading and the adsorption strength, respectively. A similar model for a material with two types of adsorption sites yields:

$$q = \frac{q_{\max,1} K_{a,1} \cdot p}{1 + K_{a,1} \cdot p} + \frac{q_{\max,2} K_{a,2} \cdot p}{1 + K_{a,2} \cdot p}, \quad (6)$$

⁷Langmuir was awarded the Nobel Prize in Chemistry 1932 for this work.

with parameters for maximum loading and adsorption strength on each type of site. The parameters in (5) and (6) fit experimental data using linear or nonlinear regression, and depend on the material, gas, and temperature.

We used data from [31] for methane adsorption on mica at 90 K, and also data from [44, Table 1] for isobutane adsorption on silicalite at 277 K. In both cases, observed values of q are given for specific values of p ; the goal is to express q as a function of p . We give the SR-module the operators $\{+, -, \times, \div\}$, and obtain the best fitting functions with two and four constants. The code ran for 20 minutes on 45 cores, and seven of these functions are displayed for each dataset.

To encode the background theory, following Langmuir's original theory [31] we elicited the following set \mathcal{A} of axioms:

| | |
|-----------------------------|---|
| L1. Site balance: | $S_0 = S + S_a$ |
| L2. Adsorption rate model: | $r_{\text{ads}} = k_{\text{ads}} \cdot p \cdot S$ |
| L3. Desorption rate model: | $r_{\text{des}} = k_{\text{des}} \cdot S_a$ |
| L4. Equilibrium assumption: | $r_{\text{ads}} = r_{\text{des}}$ |
| L5. Mass balance on q | $q = S_a$ |

Here, S_0 is the total number of sites, of which S are unoccupied and S_a are occupied (L1). The rate of adsorption r_{ads} is proportional to the pressure p and the number of unoccupied sites (L2). The rate of desorption r_{des} is proportional to the number of occupied sites (L3). At equilibrium, $r_{\text{ads}} = r_{\text{des}}$ (L4), and the total amount adsorbed, q , is the number of occupied sites (L5) because the model assumes each site accommodates at most one adsorbed molecule. Langmuir solved these equations to obtain:

$$q = \frac{S_0 * (k_{\text{ads}}/k_{\text{des}}) * p}{1 + (k_{\text{ads}}/k_{\text{des}}) * p}. \quad (7)$$

where the maximum loading q_{max} is the total number of sites, and the equilibrium constant K_a is the ratio between rate constants for adsorption and desorption. An axiomatic formulation for the multi-site Langmuir expression is described in the Appendix.

Additionally, constants and variables are constrained to be positive, e.g., $S_0 > 0$, $S > 0$, and $S_a > 0$, or non-negative, e.g., $q \geq 0$. The logic formulation is:

$$(\mathcal{C} \wedge \mathcal{A}) \rightarrow f, \quad (8)$$

where \mathcal{C} is the conjunction of the non-negativity constraints, \mathcal{A} is a conjunction of the formulas of the axioms, and f is the formula we wish to prove, e.g., (10).

SR can only generate numerical expressions involving the variables occurring in input data, with certain values for constants, e.g., the expression $f = p/(0.709 \cdot p + 0.157)$,

instead of expressions built from variables and constants from the background theory, such as (10). Moreover, (10) involves the constants k_{ads} and k_{des} , but SR only generates a numerical instance of the ratio of these constants. Thus, we cannot use (8) directly to prove equations generated from SR. Instead, we replace each numerical constant of the formula by a logic variable c_i ; e.g., the formula $f = p/(0.709 \cdot p + 0.157)$ is replaced by $f' = p/(c_1 \cdot p + c_2)$, introducing two new variables c_1 and c_2 . We then quantify the new variables existentially, and define a new set of non-negativity constraints \mathcal{C}' . In the example above we will have $\mathcal{C}' = c_1 > 0 \wedge c_2 > 0$.

The final formulation is:

$$\exists c_1 \dots \exists c_n. ((\mathcal{C} \wedge \mathcal{A}) \rightarrow (f' \wedge \mathcal{C}')). \quad (9)$$

For example, $f' = p/(c_1 \cdot p + c_2)$ is proved true if the reasoner can prove that there exist values of c_1 and c_2 (which can be functions of constants k_{ads} , k_{des} , S_0 , and/or real numbers, but not variables such as q or p) such that f' satisfies the background theory \mathcal{A} and the constraints \mathcal{C} .

We also consider background knowledge in the form of a list of desired properties of the relation between p and q , which helps trimming the set of candidate formulas. Thus, we define a collection \mathcal{K} of constraints on f , where $q = f(p)$, enforcing monotonicity or certain types of limiting behavior (see Appendix). We use Mathematica [3] to verify that a candidate function satisfies the constraints in \mathcal{K} .

In Table 2, column 1 gives the data source, and column 2 gives the “hyperparameters” used in our SR experiments: we allow either two or four constants in the derived expressions. Furthermore, as the first constraint C1 can be modeled by simply adding the data point $p = q = 0$, we also experiment with an “extra point,” though we can only work with the approximation $p = q = 0.001$. Column 3 displays a derived expression, while the columns 4 and 5 give, respectively, the relative numerical error calculated using ℓ_2 and ℓ_∞ norms. If the expression can be derived from our background theory, then we indicate that in the column 6. These results are visualized in Figure 3. Column 7 indicates the number of constraints from \mathcal{K} that each expression satisfies, verified by Mathematica. Among the first three expressions, the first two fit the data better than the third, which is derivable from the background theory, whereas the first two are not. Langmuir obtained, experimentally, $q_{\text{max}} = 108.0$ and $K_a = 0.123$ in (5) for this dataset, i.e., $q = (108 \times 0.123)p/(0.123p + 1) \approx q/(0.0926p + 0.0753)$ (if we round to three significant digits after dividing the numerator and the denominator of the first expression by $q_{\text{max}} \cdot K_a$). The constants in the third expression yield a marginally better numerical error. When we allow four constants in the derived expressions, we get much smaller errors than (5) or even (6) with the numerical parameters chosen by Langmuir, but we do not obtain

the two-site formula (6) as a candidate expression. For the dataset from Sun et al. [44], the second candidate symbolic expression has a form equivalent to Langmuir’s one-site formula, and the fifth and seventh have a form equivalent to Langmuir’s two-site formula (with appropriate values of $q_{\max,i}$ and $K_{a,i}$ for $i = 1, 2$). Furthermore, we also identify the well-known quadratic isotherm, but proving this using KeYmaera is not yet possible, as its proof requires statistical mechanics, invoking operators not available in KeYmaera [36].

| 1 | 2 | 3 | 4 | 5 | 6 | 7 |
|--------------------------|-------------------------|--|-----------------|---------------|-------------|-----------------------|
| Data | Condition | Candidate formula | Numerical Error | | | \mathcal{K} constr. |
| | | $q =$ | ℓ_2 | ℓ_∞ | provability | |
| Langmuir [31, Table IX] | 2 const. | $f_1 : (p^2 + 2p - 1) / (.00888p^2 + .118p)$ | .06312 | .04865 | timeout | 2/5 |
| | | $f_2 : p / (.00927p + .0759) *$ | .1799 | .1258 | Yes | 5/5 |
| | 4 const. | $f_3 : (p^2 - 10.5p - 15) / (.00892p^2 - 1.23)$ | .04432 | .02951 | timeout | 2/5 |
| | | $f_4 : (8.86p + 13.9) / (.0787p + 1)$ | .06578 | .04654 | No | 4/5 |
| | | $f_5 : p^2 / (.00895p^2 + .0934p - .0860)$ | .07589 | .04959 | No | 2/5 |
| | 4 const. extra-point | $f_6 : (p^2 + p) / (.00890p^2 + .106p - .0311)$ | .06833 | .04705 | timeout | 2/5 |
| | | $f_7 : (112p^2 - p) / (p^2 + 10.4p - 9.66)$ | .07708 | .05324 | timeout | 3/5 |
| Sun et al. [44, Table 1] | 2 const. | $g_1 : (p + 3) / (.584p + 4.01)$ | .1625 | .1007 | No | 4/5 |
| | | $g_2 : p / (.709p + .157)$ | .9680 | .5120 | Yes | 5/5 |
| | 4 const. | $g_3 : (.0298p^2 + 1) / (.0185p^2 + 1.16) - .000905/p^2$ | .1053 | .05383 | timeout | 2/5 |
| | | $g_4 : 1 / (p^2 + 1) + (2.53p - 1) / (1.54p + 2.77)$ | .1300 | .07247 | timeout | 3/5 |
| | 4 constants extra-point | $g_5 : (1.74p^2 + 7.61p) / (p^2 + 9.29p + 0.129)$ | .1119 | .0996 | timeout | 5/5 |
| | | $g_6 : (.226p^2 + .762p - 7.62 * 10^{-4}) / (.131p^2 + p)$ | .1540 | .09348 | timeout | 2/5 |
| | | $g_7 : (4.78p^2 + 26.6p) / (2.71p^2 + 30.4p + 1.)$ | .1239 | .1364 | timeout | 5/5 |

Table 3: Results on two datasets for the Langmuir problem. The first dataset is from Table IX in Langmuir’s paper giving observed loading of methane on mica at 90°K at different pressures. (*This expression is also generated when using four constants, and also when an extra point approximating (0, 0) is added).

We have demonstrated the value of combining logical reasoning with symbolic regression in obtaining meaningful symbolic models of physical phenomena in the sense that they are consistent with background theory and generalize well in a domain that is significantly larger than the experimental data. The synthesis of regression and reasoning yields better models than can be obtained by SR or logical reasoning alone. Improvements in individual system components and introduction of new modules (abductive reasoning, experimental design, etc.) are likely to extend the capabilities of the overall system. A

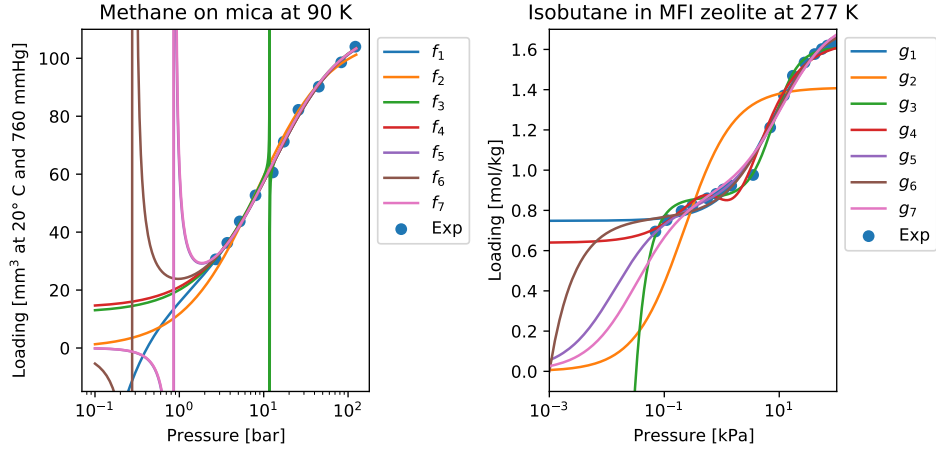


Figure 3: Symbolic regression solutions to two adsorption datasets. f_2 and g_2 are equivalent to the single-site Langmuir equation; g_5 and g_7 are equivalent to the two-site Langmuir equation.

deeper integration of reasoning and regression can help synthesize data-driven and first-principles based models, and lead to a revolution in the scientific discovery process. The discovery of models which are consistent with prior knowledge will accelerate scientific discovery, and enable going beyond existing discovery paradigms.

Datasets

Kepler's third law of planetary motion

| normalization factors | | | | |
|-----------------------|-------|-----------------------------------|-----------------------------------|--------------------------------------|
| Original | Solar | Exoplanet | Binary Stars | |
| P | [s] | $1000 \cdot 24 \cdot 60 \cdot 60$ | $1000 \cdot 24 \cdot 60 \cdot 60$ | $365 \cdot 24 \cdot 60 \cdot 60$ [y] |
| m_1 | [kg] | $1.9885 \cdot 10^{30}$ | $1.9885 \cdot 10^{30}$ | $1.9885 \cdot 10^{30}$ |
| m_2 | [kg] | $5.972 \cdot 10^{24}$ | $1.898 \cdot 10^{27}$ | $1.9885 \cdot 10^{30}$ |
| d | [m] | $1.496 \cdot 10^{11}$ [au] | $1.496 \cdot 10^{11}$ [au] | $1.496 \cdot 10^{11}$ [au] |

Table 4: Units of measurement and normalization factors for Kepler data

We use three different datasets. The first has eight data points corresponding to the eight planets of the solar system. The second has 20 data points consisting of all eight data points from the first dataset, and, in addition, data points corresponding to some exoplanets in the Trappist-1 and the GJ 667 systems. The third consists of data on five binary stars [38]. All three datasets consist of real measurements of four variables: the distance d between two bodies, a star and an orbiting planet in the first two datasets and binary stars in the third dataset, the masses m_1 and m_2 of the two bodies, and the orbital period P , which is our target variable. We normalized the data to reduce errors that can arise due to processing large numbers in our system. Table 4 gives the original unit of measurement and the normalization factors for each dataset. Each star mass is given as a multiple of the mass of the sun, hence the sun mass equals 1. In the first dataset, each planetary mass is given as a multiple of Earth's mass, whereas in the second dataset each planetary mass is given relative to Jupiter's mass. The distance d is given in astronomical units [au]. The period P is given as days/1000 or years.

Relativistic time dilation

We give one data set used in [13, Figure 2] and kindly provided to us by the first author, Dr. Chou. We report the data in Table 6. The first column gives the velocity of a moving clock relative to another stationary clock, and the second column gives the relative change in clock rates (i.e., it gives the clock rate (or frequency) of the moving clock minus the clock rate of the stationary clock divided by the clock rate of the stationary clock) scaled by 10^{15} .

We next list and describe the axioms given as input to the reasoning module for this problem. See Figure 4. The period dt_0 of a “light clock” is defined as the time for light (at

| Solar | | | | Exoplanet | | | | Exoplanets (contd.) | | | |
|-------|--------------|---------|--------|-----------|----------|---------|-----------|---------------------|--------|--------|-----------|
| m_1 | m_2 | d | t | m_1 | m_2 | d | t | m_1 | m_2 | d | t |
| 1.0 | 0.0553 | 0.3870 | 0.0880 | 1.0 | 0.000174 | 0.3870 | 0.0880 | 0.08 | 0.0043 | 0.0152 | 0.0024218 |
| 1.0 | 0.815 | 0.7233 | 0.2247 | 1.0 | 0.00256 | 0.7233 | 0.2247 | 0.08 | 0.0013 | 0.0214 | 0.0040496 |
| 1.0 | 1.0 | 1.0 | 0.3652 | 1.0 | 0.00315 | 1.0 | 0.3652 | 0.08 | 0.002 | 0.0282 | 0.0060996 |
| 1.0 | 0.107 | 1.5234 | 0.6870 | 1.0 | 0.000338 | 1.5234 | 0.6870 | 0.08 | 0.0021 | 0.0371 | 0.0092067 |
| 1.0 | 317.83 | 5.2045 | 4.331 | 1.0 | 1.0 | 5.2045 | 4.331 | 0.08 | 0.0042 | 0.0451 | 0.0123529 |
| 1.0 | 95.16 | 9.5822 | 10.747 | 1.0 | 0.299 | 9.5822 | 10.747 | 0.08 | 0.086 | 0.063 | 0.018767 |
| 1.0 | 14.54 | 19.2012 | 30.589 | 1.0 | 0.0457 | 19.2012 | 30.589 | | | | |
| 1.0 | 17.15 | 30.0475 | 59.800 | 1.0 | 0.0540 | 30.0475 | 59.800 | | | | |
| | | | | 0.33 | 0.018 | 0.0505 | 0.0072004 | | | | |
| | Binary stars | | | 0.33 | 0.012 | 0.125 | 0.02814 | | | | |
| 0.54 | 0.50 | 107.270 | 1089.0 | 0.33 | 0.008 | 0.213 | 0.06224 | | | | |
| 1.33 | 1.41 | 38.235 | 143.1 | 0.33 | 0.008 | 0.156 | 0.039026 | | | | |
| 0.88 | 0.82 | 113.769 | 930.0 | 0.33 | 0.014 | 0.549 | 0.2562 | | | | |
| 3.06 | 1.97 | 131.352 | 675.5 | 0.08 | 0.0027 | 0.0111 | 0.0015109 | | | | |

Table 5: Kepler data

| Velocity (m/s) | Time dilation (10^{-15}) |
|----------------|------------------------------|
| 0.55 | -0.018 |
| 4.10 | -0.21 |
| 8.60 | -0.43 |
| 14.84 | -1.54 |
| 22.18 | -2.92 |
| 29.65 | -4.82 |
| 36.22 | -7.36 |

Table 6: Time dilation data

velocity c) to travel between two stationary mirrors separated by distance d (axiom R1 below). The period dt of a similar pair of mirrors moving with velocity v (axiom R2), is the time taken for light to bounce between the two mirrors, but in this case, while traveling the distance L (calculated via the Pythagoras' theorem in axiom R3). The observed change in clock frequency due to motion, $df = f - f_0$, (axiom R6) is related to periods dt_0 and dt using definitions of frequency (axioms A4 and R5). The second column of the previous table gives values for df/f_0 (after scaling by 10^{15}). Here all variables are positive, and the speed of light is taken to be 3×10^8 meters per second (axioms R7-R8). In the figure below, the dashed lines represent lengths, the solid lines represent the direction of travel for light (if vertical or diagonal), or the direction of motion of the light source (horizontal).

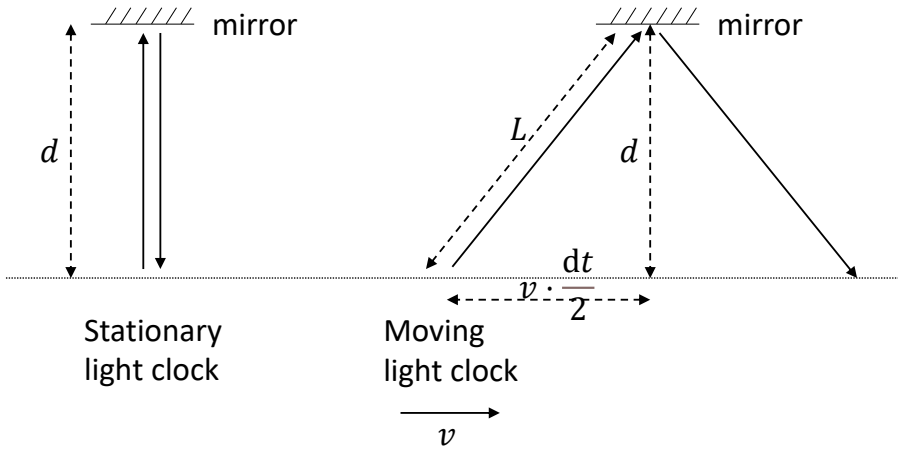


Figure 4: Depiction of moving light clock

| | |
|------------------------------------|--|
| R1. $dt_0 = 2 \cdot d/c$ | R1'. $dt_0 = 2 \cdot d/c$ |
| R2. $dt = 2 \cdot L/c$ | R2'. $dt = 2 \cdot L/\sqrt{v^2 + c^2}$ |
| R3. $L^2 = d^2 + (v \cdot dt/2)^2$ | R3. $L^2 = d^2 + (v \cdot dt/2)^2$ |
| R4. $f_0 = 1/dt_0$ | R4'. $f_0 = 1/dt_0$ |
| R5. $f = 1/dt$ | R5'. $f = 1/dt$ |
| R6. $df = f - f_0$ | R6'. $df = f - f_0$ |
| R7. $d > 0, v > 0$ | R7'. $d > 0, v > 0$ |
| R8. $c = 3 \times 10^8$ | R8'. $c = 3 \times 10^8$ |

Table 7: Axioms for relativistic time dilation are given in the first two columns, and an alternate set of axioms for "Newtonian behavior" in columns three and four.

Langmuir's adsorption equation

Data

We give two datasets, one taken from Langmuir's original paper [31, Table IX], and the other from [44, Table 1]. Each dataset gives the measured loading q at different values of pressure p at a fixed temperature. We note that different scales for pressure and loading are used in these two datasets.

| Langmuir [31, Table IX] | | Sun et al. [44, Table 1] | | | |
|-------------------------|-------|--------------------------|-------|-------|-------|
| p | q | p | q | p | q |
| 2.7 | 30.6 | 0.07 | 0.695 | 12.06 | 1.371 |
| 3.7 | 36.3 | 0.11 | 0.752 | 17.26 | 1.469 |
| 5.2 | 43.7 | 0.20 | 0.797 | 27.56 | 1.535 |
| 8.0 | 52.7 | 0.31 | 0.825 | 41.42 | 1.577 |
| 12.8 | 60.6 | 0.56 | 0.860 | 55.20 | 1.602 |
| 17.3 | 71.2 | 0.80 | 0.882 | 68.95 | 1.619 |
| 25.8 | 82.2 | 1.07 | 0.904 | 86.17 | 1.632 |
| 45.0 | 90.2 | 1.46 | 0.923 | | |
| 83.0 | 98.6 | 3.51 | 0.976 | | |
| 122.0 | 104.0 | 6.96 | 1.212 | | |

Table 8: Langmuir data

Thermodynamic constraints

A different form of background knowledge is also available for adsorption thermodynamics; equations for single-component adsorption are more plausible when they satisfy certain thermodynamic constraints \mathcal{K} :

- C1. $f(0) = 0$
- C2. $(\forall p > 0) (f(p) > 0)$
- C3. $(\forall p > 0) (f'(p) \geq 0)$
- C4. $0 < \lim_{p \rightarrow 0} f'(p) < \infty$
- C5. $0 < \lim_{p \rightarrow \infty} f(p) < \infty$

C1 requires that at zero pressure, zero molecules may be adsorbed, and C2 requires that only positive loadings are feasible. C3 requires the isotherm increase monotonically with pressure, which holds for all single-component adsorption systems. C4 requires the slope of the adsorption isotherm in the limit of zero pressure (the adsorption second virial

coefficient) to be positive and finite [45]. C5 requires the loading to be finite in the limit of infinite pressure, thus imposing a saturation capacity for the material. These five constraints are satisfied by Langmuir and multi-site Langmuir models, but some popular models in the literature violate these to various degrees. For example, Freundlich and Sips equations violate constraint C4 – a well-known issue critiqued by [45]. The BET isotherm violates C2 and C3 because of its singularity at the vapor pressure of the fluid p_{vap} ; this could be resolved by instead enforcing positivity and monotonicity from $0 < p < p_{\text{vap}}$.

Materials and Methods

Additional related work

Symbolic discovery of equations is a well studied research field, and it is a recognised challenge for the entire Artificial Intelligence community [27].

We addressed the most relevant literature in the introduction. Some other papers worth mentioning are at the intersection of symbolic discovery and deep learning. Several attempts have been made to use deep neural networks for learning or discovering symbolic equations [34, 30, 24, 4, 22, 25, 16]. For example, in [25] the authors focused on modelling a neural network architecture on the human physical reasoning process. In [4] the authors use tree LSTMs to incorporate the structure of the symbolic expression trees, and combine symbolic reasoning and function evaluation for solving the tasks of equation verification and equation completion. Symbolic regression has been used in [16] to extract explicit physical relations from components of the learned model of a Graph Neural Network (GNN). In [18], the authors employ symbolic regression to construct parsimonious process models described by analytic equations for real-time RL control when dealing with unknown or time-varying dynamics. In [47] (and the subsequent paper AI-Feynman 2.0 [46]), the authors introduce a recursive multidimensional symbolic regression algorithm that combines neural network fitting with a suite of physics-inspired techniques to find an equation that matches data from an unknown function. In [26], symbolic regression is combined with Bayesian models. Moreover, neuro-symbolic systems have received a lot of attention in the past years: see the papers on combining mathematical reasoning with deep neural networks [32, 12]. Bayesian program synthesis has also been successful for learning a “library” of equations. Other types of search have been investigated as well, e.g., Bayesian Markov Chain Monte Carlo search [23], graph-based search [37], or methods for identifying linear combinations of nonlinear descriptors for dynamic systems (SINDy). However, to the best of our knowledge, these methods have never been combined with logical reasoning.

Symbolic regression

For details on the symbolic regression solver based on a novel MINLP formulation that we use for our system see:

- V. Austel, C. Cornelio, S. Dash, J. Goncalves, L. Horesh, T. R. Josephson, N. Megiddo, *Symbolic regression using mixed-integer nonlinear optimization*, CoRRabs 2006.06813 (2020). <https://arxiv.org/abs/2006.06813>.

Reasoning and Derivability

Logic and Reasoning Background

We assume the reader has knowledge of basic first-order logic and automated theorem proving terminology and thus will only briefly describe the terms commonly seen throughout this paper. For readers interested in learning more about logical formalisms and techniques see [11, 19].

In this work, we focus on first-order logic (FOL) with equality. In the standard FOL problem-solving setting, an ATP (automated theorem prover) is given a *conjecture* (i.e., a formula to be proved true or false) and *axioms* (i.e., formulas known to be true). The set of axioms is also called *background theory*. From these inputs, the ATP performs a *derivation*, which can be characterized as the successive application of inference rules (i.e., rules that, based on given true formulas, allow for the derivation of new true formulas) to axioms and derived formulas until a *proof* of the given conjecture is found. The set of *derivable formulas* from a background theory is the set of logic formulas that can be derived from the set of axioms defining the background theory.

All formulas considered in this work are in FOL formulas with equality and basic arithmetic operators, i.e., defined based on the FOL grammar with the addition of the function symbols for equality $=$, inequality $>$, $<$, sum $+$, subtraction $-$, product $*$, division $/$ and power $^$ (the square root is interpreted as a power of $\frac{1}{2}$).

First-order logic formulae are formal expressions based on an alphabet of predicates, functions, and variable symbols which are combined by logical connectives. A term is either a variable, a constant (function with no arguments), or, inductively, a function applied to a tuple of terms. A formula is either a predicate applied to a tuple of terms or, inductively, a connective (e.g., \wedge read as “and”, \vee as “or”, \neg as negation, etc.) applied to some number of formulae. In addition, variables in formulae can be universally or existentially quantified (i.e., by the quantifiers \forall and \exists which read as “for all” and “exists” respectively), where a quantifier introduces a semantic restriction for the interpretation of the variables it quantifies.

KeYmaeraX

Reasoning tools for arithmetic and calculus that, in principle, have the required logic capabilities of checking consistency, validation, and deduction include: SymPy [35], Prolog [2], Mathematica [3], Beagle [9], and KeYmaera [21, 1].

We integrated in our system several reasoning tools for arithmetic and calculus, analyzing their expressiveness and capabilities (including, but not only, the one mentioned above). Our findings made us decide in favour of the KeYmaeraX reasoner: an automated theorem prover for hybrid systems that combines different types of reasoning: deductive, real algebraic, and computer algebraic reasoning.

The underlying logic supported by KeYmaera is differential dynamic logic [40], which is a real-valued first-order dynamic logic for hybrid programs. KeYmaera is based on a generalized free-variable sequent calculus inference rule for deductive reasoning and has an underlying CAD system (e.g. Mathematica).

KeYmaeraX provides fast computation for first-order logic formulas combined with arithmetic and differential equations, even though it does not provide full explainability for the derivations: only the final state (provable/not-provable) is available while the proof-steps are not.

KeYmaeraX formulation for Kepler's third law

We first consider the KeYmaera formulation⁸ for the ℓ_∞ norm. As example, we consider for $f(\mathbf{x})$ corresponding to $P_N = \sqrt{0.1319 \cdot d_N^3}$ extracted via SR from the solar system dataset. We compute the error between and \tilde{f} represented by P_N , which is the normalized variable⁹ corresponding to the orbital period.

```

1  Problem (( m1>0 & m2>0 & P>0 & d2>0 & d1>0 & m1N>0 & m2N>0 & PN>0
2    & G = (6.674 * 10^(-11)) & pi = (3.14) & err = 10^-2
3    & ( m1 * d1 = m2 * d2 )
4    & ( d = d1 + d2 )
5    & ( Fg = (G * m1 * m2) / d^2 )
6    & ( Fc = m2 * d2 * w^2 )
7    & ( Fg = Fc )
8    & ( P = (2 * pi) / w )
9    & convP = (1000 * 24 * 60 * 60 )
10   & convm1 = (1.9885 * 10^30 )
11   & convm2 = (5.972 * 10^24)
12   & convD = (1.496 * 10^11)

```

⁸In what follows we omit Variables and Definitions for simplicity

⁹We add the suffix N to the variables after they have been normalized (e.g., $m1$ become $m1_N$, d become d_N , etc.).

```

13  & m1N = m1 / convm1
14  & m2N = m2 / convm2
15  & dN = d / convD
16  & PN = P / convP
17 )->(((m1N=1 & m2N=0.055 & dN=0.3871) -> abs((0.1319 * dN^3 )^(1/2) - (PN))/PN < err)
18  & ((m1N=1 & m2N=0.815 & dN=0.7233) -> abs((0.1319 * dN^3 )^(1/2) - (PN))/PN < err)
19  & ((m1N=1 & m2N=1 & dN=1) -> abs((0.1319 * dN^3 )^(1/2) - (PN))/PN < err)
20  & ((m1N=1 & m2N=0.107 & dN=1.5237) -> abs((0.1319 * dN^3 )^(1/2) - (PN))/PN < err)
21  & ((m1N=1 & m2N=317.8 & dN=5.2044) -> abs((0.1319 * dN^3 )^(1/2) - (PN))/PN < err)
22  & ((m1N=1 & m2N=95.159 & dN=9.5826) -> abs((0.1319 * dN^3 )^(1/2) - (PN))/PN < err)
23  & ((m1N=1 & m2N=14.536 & dN=19.2184) -> abs((0.1319 * dN^3 )^(1/2) - (PN))/PN < err)
24  & ((m1N=1 & m2N=17.147 & dN=30.07) -> abs((0.1319 * dN^3 )^(1/2) - (PN))/PN < err)
25 ) ) End.

```

In particular we see that:

- **line 1** describes feasibility constraints, e.g., the masses only admit positive values;
- **line 2** defines some constants such as the gravitational constant, the value of π , and the error bound ($err = 10^{-2}$);
- **lines 3-8** are the axioms of the background theory;
- **lines 9-16** are the normalization specifications (e.g. m_{1N} is the normalized variable corresponding to the mass m_1)
- **lines 17-24** contain the specification of the ℓ_∞ norm: given each data point (instantiation of the value of the two masses and their relative distance) we want to prove that the distance between the formula induced from the data (in this case $P_N = \sqrt{0.1319 \cdot d_N^3}$) and the actual formula deducible from the axioms for P_N is smaller than the value of err . In this way, if all the data points respect the error bound, the max value will as well.

KeYmaera is able to produce a successful proof of the formulation above for an error bound of $err = 10^{-2}$.

The value for the generalization reasoning error (ℓ_∞ norm) is computed by using binary search over the values of the relative error $abs((0.1319 * dN^3)^(1/2) - (PN))/PN$. In these experiments we used a time limit of 1200 seconds (20 min) and stopped the binary search process when a precision of 10^{-4} is attained.

The formulation for ℓ_2 norm is very similar, with the difference that the binary search is performed over the single data points as described in Algorithm 1, where

$$\min_e \{ \text{KeYmaera}\ell_2(i, e) \mid \text{precision} \}$$

computes an upperbound on the minimum value for e for a give precision level (which is 10^{-4} in the experiments) such that $\text{KeYmaera}\ell_2(i, e)$ returns *true*. This is necessary because KeYmaera is fundamentally a boolean function, mapping formulations to a success/failure state and is thus not able to perform optimization over continuous values. The function $\min_e \{\text{KeYmaera}(e)\}$ is therefore calculated approximately (via binary search) in a given interval with a input precision level and fixing a time limit (20 min in the experiments).

Algorithm 1 ℓ_2 norm computed with KeYmaera

```

1: procedure  $\ell_2(\text{Dataset})$ 
2:   for  $i$  in  $\text{Dataset}$  do
3:      $e_i \leftarrow \min_e \{\text{KeYmaera}\ell_2(i, e) \mid \text{precision}\}$ 
4:    $\ell_2 \leftarrow \sqrt{e_1^2 + \dots + e_n^2}$ 

```

The KeYmaera formulation for $\text{KeYmaera}\ell_2(i, e)$ on a specific data point i and an error bound e is a Boolean function that returns *true* if the following program is provable and *false* otherwise. $\text{KeYmaera}\ell_2(i, e)$ returns *true* when, for a given set of axioms, the absolute value of the relative distance between a given function and a deducible one is smaller than e for a given data point i . For example, given the data point $(m_{1N}, m_{2N}, d_N) = (1, 0.055, 0.3871)$ and error $e = 10^{-2}$ we have the following formulation:

```

1  Problem (( m1>0 & m2>0 & P>0 & d2>0 & d1>0 & m1N>0 & m2N>0 & PN>0
2    & G = (6.674 * 10^(-11)) & pi = (3.14) & e = 10^-2
3    & ( m1 * d1 = m2 * d2 )
4    & ( d = d1 + d2 )
5    & ( Fg = (G * m1 * m2) / d^2 )
6    & ( Fc = m2 * d2 * w^2 )
7    & ( Fg = Fc )
8    & ( P = (2 * pi) / w )
9    & convP = (1000 * 24 * 60 * 60 )
10   & convm1 = (1.9885 * 10^30 )
11   & convm2 = (5.972 * 10^24)
12   & convD = (1.496 * 10^11)
13   & m1N = m1 / convm1
14   & m2N = m2 / convm2
15   & dN = d / convD
16   & PN = P / convP
17   )->(((m1N=1 & m2N=0.055 & dN=0.3871) -> abs((0.1319 * dN^3 )^(1/2) - (PN))/PN < e)
18 ) ) End.

```

We observed that the point-wise reasoning errors are not very informative if SR yields

a low-error candidate expression (measured with respect to the data), and the data itself satisfies the background theory up to a small error, which indeed is the case with the data we use; the reasoning errors and numerical errors are very similar. This is true because if we can evaluate the numerical error, i.e., we have data for the real values of P_N , then we may assume that the error of the candidate formula at the data points is substantially equal to the error of the correct formula. In particular, this is true when the data is generated synthetically like in [47].

However, this analysis is still relevant if we wish to evaluate the error in the data:

$$\text{Error in the data} = \text{Numerical error} - \text{Reasoning error}.$$

The latter is useful for avoiding overfitting entailed in formulas with numerical error smaller than error in the data.

Let's consider again the formula $f(\mathbf{x}) = \sqrt{0.1319 \cdot d_N^3}$ (extracted via SR from the solar system dataset) for the variable of interest P_N . The KeYmaera formulation for the generalization reasoning error is the following:

```

1 Problem (( P>0 & PN>0
2   & G = (6.674 * 10^(-11)) & pi = (3.14) & err = 10^-6
3   & m1N>=0.08 & m1N<=1
4   & m2N>=0.0002 & m2N<=1
5   & dN>=0.0111 & dN<=30.1104
6   & ( m1 * d1 = m2 * d2 )
7   & ( d = d1 + d2 )
8   & ( Fg = (G * m1 * m2) / d^2 )
9   & ( Fc = m2 * d2 * w^2 )
10  & ( Fg = Fc )
11  & ( P = (2 * pi) / w )
12  & convP = (1000 * 24 * 60 * 60 )
13  & convm1 = (1.9885 * 10^30 )
14  & convm2 = (5.972 * 10^24)
15  & convD = (1.496 * 10^11)
16  & m1N = m1 / convm1
17  & m2N = m2 / convm2
18  & dN = d / convD
19  & PN = P / convP
20 )->((abs(0.1319 * dN^3 )^(1/2) - PN ) / (PN) < err ))
21 End.

```

In particular we have that:

- line 1 describes feasibility constraints;

- **line 2** defines some constants such as the gravitational constant, π value and the error bound;
- **lines 3-5** define the intervals for the variables, extracted from the dataset normalized data points (e.g. the planets in the solar system have a distance more than 0.0111 astronomical units and less than 30.1104 astronomical units from the sun);
- **lines 6-11** are the axioms of the background theory;
- **lines 12-19** are the normalization specifications;
- **lines 17-24** contain the specification of the error: given each data point (instantiation of the value of the two masses and their relative distance) we want to prove that the distance between the formula induced from the data (in this case $P_N = \sqrt{0.1319 \cdot d_N^3}$) and the actual formula deducible from the axioms for P_N is smaller than the value of err .

KeYmaera formulation for Relativistic time dilation

We give a formulation to check for the quality of generalization for a given formula, in particular, the function $y = -0.00563v^2$ computed from data. The velocity of light c is given as a fixed constant 3×10^8 (meters per second). The ℓ_∞ error is bounded above by 1. The formulation asserts that there is a derivable formula that differs (after scaling by 10^{15}) from the function $-0.00563v^2$ by at most 1 in the domain $37 \leq v \leq 115$.

```

1 Problem((d > 0 & L > 0 & c = 3*10^8 & err = 1
2   & v >= 37 & v <= 115
3   & dt0 = 2*d/c
4   & L^2 = d^2 + (v*dt/2)^2
5   & dt = 2*L/c
6   & f0 = 1/dt0
7   & f = 1/dt
8   & df = f - f0
9   & y = 10^15*df/f0 )
10  -> ( ( abs( (-0.00563)*(v^2)) - y < err ) ) )
11 End.

```

KeYmaeraX formulation for proving Langmuir's adsorption equation

The KeYmaeraX formulation to prove the Langmuir equation:

$$q = \frac{S_0 \cdot (k_{\text{ads}}/k_{\text{des}}) \cdot p}{1 + (k_{\text{ads}}/k_{\text{des}}) \cdot p}. \quad (10)$$

from the background theory described in the manuscript (L1–L5) is the following:

```

1 Definitions
2   Real kads;
3   Real kdes;
4   Real S0;
5 End.
6 Problem
7  ( \forall Q \forall S \forall Sa \forall P \forall rdes \forall rads(
8      (kads>0 & kdes>0 & S0>0 & Q>0 & S>0 & Sa>0 & P>0 & rdes>0 & rads>0
9      & S0 = S + Sa
10     & rads = kads * P * S
11     & rdes = kdes * Sa
12     & rads = rdes
13     & Q = Sa)
14  -> Q = ((S0 * (kads / kdes)) * P) / (1 + ((kads / kdes)*P) ) )
15 End.

```

This formulation is successfully proved by KeYmaera.

As expected, when removing one or more axioms that are strictly necessary to prove the theorem (e.g., the axiom $r_{\text{des}} = k_{\text{des}} \cdot S_a$), it is not possible to prove the equation anymore. Similarly, if f does not correspond to the correct formula (while the axiom set is complete and correct) KeYmaera is not able to provide a provability certification. In this case it is possible to create a numerical counterexample (a numerical assignment to all the variables involved in the problem formalization, that falsify the implication). Moreover, it is possible to add additional constraints and assumptions to generate further counterexamples.

An example of a counterexample, obtained by removing an essential (to prove the theorem) axiom from the background theory (the axiom $r_{\text{des}} = k_{\text{des}} \cdot S_a$), is the following:

$$[Q, S, P, S_0, r_{\text{des}}, S_a, k_{\text{des}}, k_{\text{ads}}r_{\text{ads}}] = [1, 1, 1/2, 2, 1/2, 1, 1, 1/2]$$

It is possible to add additional constraints and assumptions to generate further counterexamples: e.g., if we exclude the value 1 for the variable Q (the assignment of Q in the previous counterexample) adding the constraint $Q \neq 1$, the Counter-Example Search tool provides a new solution:

$$[Q, S, P, S_0, r_{\text{des}}, S_a, k_{\text{des}}, k_{\text{ads}}r_{\text{ads}}] = [1/4, 1/4, 1/2, 1/2, 1/8, 1/4, 1, 1/8]$$

Background theory for multi-site Langmuir model

Langmuir defined expressions to model adsorption onto a material that contains different kinds of sites, with different interaction strengths [31]. Consequently, we generalize the

background theory to model this scenario. Some quantities (S_a , S_0 , S , k_{ads} , k_{des} , r_{ads} , and r_{des}) now depend on the site. The axioms below, which are universally quantified over the sites, hold for each site as before, while the definition of the adsorbed amount changes to allow for the presence of multiple sites. The new set of axioms is:

- GL1. $\forall X. S_0(X) = S(X) + S_a(X)$
- GL2. $\forall X. r_{ads}(X) = k_{ads}(X) \cdot p \cdot S(X)$
- GL3. $\forall X. r_{des}(X) = k_{des}(X) \cdot S_a(X)$
- GL4. $\forall X. r_{ads}(X) = r_{des}(X)$
- GL5. $Q = \sum_{i=1}^{\infty} S_a(X)$
- GL6. $\bigwedge_{i=1}^{\infty} (St = i \rightarrow (\bigwedge_{j>i} S_0(j) = 0))$
- GL7. $\bigvee_{i=1}^{\infty} St = i$

where GL1–GL4 are as before; GL5 ensures that the total amount adsorbed is the sum of the amounts adsorbed in each site; GL6 ensures that if there are i site types ($St = i$) the types with higher index have no sites; and GL7 ensures that there is only one value for the number of site types.

We implemented an alternative KeYmaera formulation for the two-sites model:

```

1  Definitions
2  Real kads_1;
3  Real kdes_1;
4  Real S0_1;
5  Real kads_2;
6  Real kdes_2;
7  Real S0_2;
8  End.
9  ProgramVariables
10 Real Q;
11 Real S_1;
12 Real S_2;
13 Real Sa_1;
14 Real Sa_2;
15 Real P;
16 Real rdes_1;
17 Real rads_1;
18 Real rdes_2;
19 Real rads_2;
20 End.
21 Problem
22 ( ( kads_1>0 & kdes_1>0 & S0_1>0 & S_1>0 & Sa_1>0 & rads_1>0 & rdes_1>0

```

```

23      & kads_2>0 & kdes_2>0 & S0_2>0 & S_2>0 & Sa_2>0 & rads_2>0 & rdes_2>0 &
24      & Q>=0 & P>0
25      & S0_1 = S_1 + Sa_1
26      & rads_1 = kads_1 * P * S_1
27      & rdes_1 = kdes_1 * Sa_1
28      & rads_1 = rdes_1
29      & S0_2 = S_2 + Sa_2
30      & rads_2 = kads_2 * P * S_2
31      & rdes_2 = kdes_2 * Sa_2
32      & rads_2 = rdes_2
33      & Q = Sa_1 + Sa_2 )
34  -> Q = (S0_1 * (kads_1 / kdes_1) * P)/(1+(kads_1/kdes_1) *P)
35  +(S0_2 * (kads_2/ kdes_2) * P)/ (1 + ((kads_2 / kdes_2) * P)))
36 End.

```

This formulation is successfully proved by KeYmaera. This formulation is equivalent to the one described for a generic number of sites, except that it duplicates variables used in the axiom system for the one-site model instead of creating dependencies on the site type. This grounding of the general formulation to the case of two sites helps the reasoner converge faster to a solution if the number of sites is small. However, this approach applied to n sites would result in an exponential growth (with n) of the number of equations and would lead to increasing computing times. In general, a more compact representation (with fewer logical/non-logical symbols) is preferred.

KeYmaeraX formulations for Langmuir's theory experiments

When the input formula (to be derived) has numerical constants, we need to introduce existentially quantified variables. For example, given an input formula $P/(0.00927 P + 0.0759)$, we first transform it to $P/(c_1 P + c_2)$ (where c_1 and c_2 are existentially quantified). The following KeYmaera formulation is used:

```

1 Definitions
2   Real kads;
3   Real kdes;
4   Real S0;
5 End.
6 Problem
7 ( \exists c1 \exists c2 \forall Q \forall S \forall Sa \forall P \forall rdes \forall rads(
8   (kads>0 & kdes>0 & S0>0 & Q>0 & S>0 & Sa>0 & P>0 & rdes>0 & rads>0
9   & S0 = S + Sa
10  & rads = kads * P * S
11  & rdes = kdes * Sa

```

```

12      & rads = rdes
13      & Q = Sa)
14  -> ( c1>0 & c2>0 & Q = P/(c1 * P +c2) ))
15 End.

```

This formulation is successfully proved by KeYmaera , however it does not provide any (symbolic or numerical) instantiation for the existentially quantified variables that satisfy the logic program. In this case, manual inspection can show that instantiating $c_1 = 1/S_0$ and $c_2 = \frac{k_{\text{des}}}{k_{\text{ads}}S_0}$ provides a valid solution. To obtain this result automatically would require an extension of KeYmaeraX (or more broadly a theorem prover) to allow for explicit variable assignments.

Likewise, the formulation for proving expressions generated by symbolic regression with the two-site Langmuir model is the following:

```

1 Definitions
2   Real kads_1;
3   Real kdes_1;
4   Real S0_1;
5   Real kads_2;
6   Real kdes_2;
7   Real S0_2;
8 End.
9 Problem
10 ( \exists c1 \exists c2 \exists c3 \exists c4 \forall Q
11   \forall S_1 \forall S_2 \forall Sa_1 \forall Sa_2 \forall P(
12     ( S_1>0 & Sa_1>0 & S0_1>0 & kads_1>0 & kdes_1>0
13     & S_2>=0 & Sa_2>=0 & S0_2>0 & kads_2>0 & kdes_2>0
14     & Q>=0 & P>0
15     & S0_1 = S_1 + Sa_1
16     & kdes_1 * Sa_1 = kads_1 * P * S_1
17     & S0_2 = S_2 + Sa_2
18     & kdes_2 * Sa_2 = kads_2 * P * S_2
19     & Q = Sa_1 + Sa_2)
20  -> (Q = (c1*P^2+c2*P)/(P^2+c3*P+c4) & c1>0 & c2>0 & c3>0 & c4>0 ))
21 End.

```

Using this formulation, KeYmaera timed out without proving or disproving any of the conjectures provided by the SR module. However, we noticed that g_5 and g_7 satisfy all the thermodynamic constraints \mathcal{K} (in contrast to the other 4-parameter formulas) and thus we tried to prove them manually. We were able to do so, obtaining the following variable instantiations: $c_1 = S_{0,1} + S_{0,2}$, $c_2 = \frac{S_{0,1}K_1 + S_{0,2}K_2}{K_1K_2}$, $c_3 = \frac{K_1 + K_2}{K_1K_2}$, and $c_4 = 1/(K_1K_2)$, where $K_i = k_{\text{ads}_i}/k_{\text{des}_i}$.

Acknowledgements We thank J. Ilja Siepmann for initially suggesting adsorption as a problem for symbolic regression. We thank James Chin-wen Chou for providing the atomic clock data. *Funding:* This work was supported in part by the Defense Advanced Research Projects Agency (DARPA) (PA-18-02-02). The U.S. Government is authorized to reproduce and distribute reprints for Governmental purposes notwithstanding any copyright notation thereon. TRJ was supported by the U.S. Department of Energy (DOE), Office of Basic Energy Sciences, Division of Chemical Sciences, Geosciences and Biosciences (DE-FG02-17ER16362), as well as startup funding from the University of Maryland, Baltimore County. TRJ also gratefully acknowledges the University of Minnesota Institute for Mathematics and its Applications (IMA).

References

- [1] Keymaera X. <http://www.cs.cmu.edu/KeYmaeraX/>. Version: 4.8.
- [2] SWI-prolog. <https://www.swi-prolog.org>. Version: 8.3.3.
- [3] Wolfram Mathematica. <https://www.wolfram.com>. Version: 12.
- [4] Forough Arabshahi, Sameer Singh, and Anima Anandkumar. Combining symbolic expressions and black-box function evaluations in neural programs. In *ICLR*, 2018.
- [5] Dhananjay Ashok, Joseph Scott, Sebastian J. Wetzel, Maysum Panju, and Vijay Ganesh. Logic guided genetic algorithms (student abstract). *Proceedings of the AAAI Conference on Artificial Intelligence*, 35(18):15753–15754, May 2021.
- [6] Douglas Adriano Augusto and Helio JC Barbosa. Symbolic regression via genetic programming. In *Proc. 6th Brazilian Symp. Neural Networks*, pages 173–178. IEEE, 2000.
- [7] Vernon Austel, Sanjeeb Dash, Oktay Gunluk, Lior Horesh, Leo Liberti, Giacomo Nannicini, and Baruch Schieber. Globally optimal symbolic regression. *NIPS Symposium on Interpretable Machine Learning*, 2017.
- [8] Boaz Barak and David Steurer. Sum-of-squares proofs and the quest toward optimal algorithms. *CoRR*, abs/1404.5236, 2014.
- [9] Peter Baumgartner, Joshua Bax, and Uwe Waldmann. Beagle – A Hierarchic Superposition Theorem Prover. In Amy P. Felty and Aart Middeldorp, editors, *CADE-25 – 25th International Conference on Automated Deduction*, volume 9195 of *LNAI*, pages 367–377, 2015.
- [10] F. Behroozi. A simple derivation of time dilation and length contraction in special relativity. *Phys. Teach.*, 52:410–412, 2014.
- [11] M. Bergmann, J. Moor, and J. Nelson. *The Logic Book*. McGraw-Hill Higher Education, 2013.
- [12] Davide Castelvecchi. AI Copernicus ‘discovers’ that earth orbits the sun. *Nature*, 575:266–267, 2019.
- [13] C. W. Chou, D. B. Hume, T. Rosenband, and D. J. Wineland. Optical clocks and relativity. *Science*, 329:1630–1632, 2010.

- [14] A. Cozad. *Data- and theory-driven techniques for surrogate-based optimization*. PhD thesis, Carnegie Mellon, Pittsburgh, PA, 2014.
- [15] Alison Cozad and Nikolaos V. Sahinidis. A global MINLP approach to symbolic regression. *Math. Program., Ser. B*, 170:97–119, 2018.
- [16] M. Cranmer, A. Sanchez-Gonzalez, P. Battaglia, R. Xu, K. Cranmer, D. Spergel, and S. Ho. Discovering symbolic models from deep learning with inductive biases. In *NeurIPS 2020: Proceedings of the 34th International Conference on Neural Information Processing Systems*, 2020.
- [17] Maxwell Crouse, Ibrahim Abdelaziz, Bassem Makni, Spencer Whitehead, Cristina Cornelio, Pavan Kapanipathi, Edwin Pell, Kavitha Srinivas, Veronika Thost, Michael Witbrock, and Achille Fokoue. A deep reinforcement learning based approach to learning transferable proof guidance strategies. In *Proceedings of the Thirty-Fifth AAAI Conference on Artificial Intelligence (AAAI-21)*, 2021.
- [18] Erik Derner, Jirí Kubalík, Nicola Ancona, and Robert Babuska. Symbolic regression for constructing analytic models in reinforcement learning. *CoRR*, abs/1903.11483, 2019.
- [19] H. Enderton and H.B. Enderton. *A Mathematical Introduction to Logic*. Elsevier Science, 2001.
- [20] Alhussein Fawzi, Mateusz Malinowski, Hamza Fawzi, and Omar Fawzi. Learning dynamic polynomial proofs. *CoRR*, abs/1906.01681, 2019.
- [21] Nathan Fulton, Stefan Mitsch, Jan-David Quesel, Marcus Völp, and André Platzer. KeYmaera X: An axiomatic tactical theorem prover for hybrid systems. In *Lecture Notes in Computer Science*, volume 9195, 08 2015.
- [22] Alex Goeßmann, M Götte, Ingo Roth, Ryan Sweke, Gitta Kutyniok, and Jens Eisert. Tensor network approaches for learning non-linear dynamical laws. In *First Workshop on Quantum Tensor Networks in Machine Learning, 34th Conference on Neural Information Processing Systems (NeurIPS 2020)*, 2020.
- [23] Roger Guimerà, Ignasi Reichardt, Antoni Aguilar-Mogas, Francesco Alessandro Massucci, Manuel Miranda, Jordi Pallarès, and Marta Sales-Pardo. A Bayesian machine scientist to aid in the solution of challenging scientific problems. *Science Advances*, 6, Jan 2020.

- [24] William H. Guss and R. Salakhutdinov. On universal approximation by neural networks with uniform guarantees on approximation of infinite dimensional maps. *ArXiv*, abs/1910.01545, 2019.
- [25] Raban Iten, Tony Metger, Henrik Wilming, Lídia Rio, and Renato Renner. Discovering physical concepts with neural networks. *Physical Review Letters*, 124, 01 2020.
- [26] Ying Jin, Weilin Fu, Jian Kang, and J. Guo. Bayesian symbolic regression. *arXiv: Methodology*, 2019.
- [27] Hiroaki Kitano. Artificial intelligence to win the nobel prize and beyond: Creating the engine for scientific discovery. *AI Magazine*, 37(1):39–49, Apr. 2016.
- [28] John R. Koza. *Genetic Programming: On the Programming of Computers by Means of Natural Selection*. MIT Press, Cambridge, 1992.
- [29] John R. Koza. *Genetic Programming II: Automatic Discovery of Reusable Programs*. MIT Press, Cambridge, 1994.
- [30] G. Lample and F. Charton. Deep learning for symbolic mathematics. *CoRR*, 2019.
- [31] Irving Langmuir. The adsorption of gases on plane surfaces of glass, mica and platinum. *J. Amer. Chem. Soc.*, 40(9):1361–1403, 1918.
- [32] D. Lee, C. Szegedy, M. N. Rabe, S. M. Loos, and K. Bansal. Mathematical reasoning in latent space. *CoRR*, 2019.
- [33] Giuseppe Marra, Francesco Giannini, Michelangelo Diligenti, and Marco Gori. Constraint-based visual generation. *arXiv:1807.09202*, 2018.
- [34] Georg Martius and Christoph H. Lampert. Extrapolation and learning equations. In *Proceedings of the 29th Conference on Neural Information Processing Systems NIPS 2016*, 2016.
- [35] Aaron Meurer, Christopher P. Smith, Mateusz Paprocki, Ondřej Čertík, Sergey B. Kirpichev, Matthew Rocklin, AMiT Kumar, Sergiu Ivanov, Jason K. Moore, Sartaj Singh, Thilina Rathnayake, Sean Vig, Brian E. Granger, Richard P. Muller, Francesco Bonazzi, Harsh Gupta, Shivam Vats, Fredrik Johansson, Fabian Pedregosa, Matthew J. Curry, Andy R. Terrel, Štěpán Roučka, Ashutosh Saboo, Isuru Fernando,

Sumith Kulal, Robert Cimrman, and Anthony Scopatz. SymPy: symbolic computing in Python. *PeerJ Computer Science*, 3:e103, January 2017. Version: 1.5.1, <https://www.sympy.org>.

- [36] Michel Moreau, Patrick Valentin, Claire Vidal-Madjar, Bing Chang Lin, and Georges Guiochon. Adsorption isotherm model for multicomponent adsorbate—adsorbate interactions. *Journal of Colloid and Interface Science*, 141(1):127–136, 1991.
- [37] Robert Munafo. RIES - find algebraic equations, given their solution.
- [38] B. Novaković. Orbits of five visual binary stars. *Baltic Astronomy*, 16:435–442, 2007.
- [39] Pablo A. Parrilo. *Structured semidefinite programs and semialgebraic geometry methods in robustness and optimization*. PhD thesis, Caltech, Pasadena, 2000.
- [40] André Platzer. Differential dynamic logic for hybrid systems. *J. Autom. Reas.*, 2008.
- [41] Michael Schmidt and Hod Lipson. Distilling free-form natural laws from experimental data. *Science*, 324(5923):81–85, 2009.
- [42] Joseph Scott, Maysum Panju, and Vijay Ganesh. LGML: Logic Guided Machine Learning. arXiv:**2006.03626**, 2021.
- [43] Glenn S. Smith. A simple electromagnetic model for the light clock of special relativity. *Eur. J. Phys.*, 32:1585–1595, 2011.
- [44] Matthew S. Sun, D. B. Shah, Heather H. Xu, and Orhan Talu. Adsorption equilibria of C1 to C4 alkanes, CO₂, and SF₆ on silicalite. *J. Phys. Chem. B*, 102:1466–1473, 1998.
- [45] Orhan Talu and Alan L. Myers. Rigorous thermodynamic treatment of gas adsorption. *AIChE Journal*, 34(11):1887–1893, 1988.
- [46] Silviu-Marian Udrescu, Andrew Tan, Jiahai Feng, Orisvaldo Neto, Tailin Wu, and Max Tegmark. AI Feynman 2.0: Pareto-optimal symbolic regression exploiting graph modularity. In Hugo Larochelle, Marc’Aurelio Ranzato, Raia Hadsell, Maria-Florina Balcan, and Hsuan-Tien Lin, editors, *Advances in Neural Information Processing Systems 33: Annual Conference on Neural Information Processing Systems 2020, NeurIPS 2020, December 6-12, 2020, virtual*, 2020.
- [47] Silviu-Marian Udrescu and Max Tegmark. AI Feynman: A physics-inspired method for symbolic regression. *Science Advances*, 2020.